Obrabotka metallov (tekhnologiya, oborudovanie, instrumenty) = Metal Working and Material Science. 2026 vol. 28 no. 3 pp. 185–204
ISSN: 1994-6309 (print) / 2541-819X (online)
DOI: 10.17212/1994-6309-2026-28.3-185-204

NSTU NETI

Obrabotka metallov - Metal Working and Material Science

Journal homepage: http://journals.nstu.ru/obrabotka_metallov

Structural characterization of graphene-coated copper substrate prepared by scalable In-Situ spray coating using xylene dispersion

Sudhakar Vitthalrao Giri [1, 2, a, *], ***Arun Autee*** [3, b], ***Abhijeet Kadam*** [4, c], ***Rajendra Shinde*** [2, d]

[1] Dr. Babasaheb Ambedkar Marathwada University, Chhatrapati Sambhajinagar, Maharashtra, 431004, India
[2] Department of Mechanical Engineering, CSMSS Chhatrapati Shahu College of Engineering, Kanchanwadi, Chhatrapati Sambhajinagar, Maharashtra, 431011, India
[3] Department of Mechanical Engineering, Maharashtra Institute of Technology, Beed Bypass Road, Satara Parisar, Gate No. 5, Chhatrapati Sambhajinagar, Maharashtra, 431010, India
[4] Department of Physics, CSMSS Chhatrapati Shahu College of Engineering, Kanchanwadi, ChhatrapatiSambhajinagar, Maharashtra, 431011, India

[a] https://orcid.org/0009-0009-0230-2030, sudhavgiri@gmail.com; [b] https://orcid.org/0000-0003-2132-0532, arun.autee@mit.asia;
[c] https://orcid.org/0000-0002-0593-6145, arkadam6@gmail.com; [d] https://orcid.org/0000-0002-5329-1118, rajendrashinde2222@gmail.com

ARTICLE INFO

Article history:
Received: 24 May 2026
Revised: 30 May 2026
Accepted: 13 June 2026
Available online: 15 September 2026

Keywords:
Graphene coating
Heat exchanger
Spray coating
Xylene dispersion
Copper substrate
Raman spectroscopy
FTIR analysis
XRD characterization
Few-layer graphene
Thermal management

ABSTRACT

Introduction. Graphene exhibits exceptional thermal conductivity, hydrophobicity, mechanical strength, and electron transport properties, which render it a candidate material for advanced thermal management and heat transfer applications. However, conventional deposition techniques, such as chemical vapor deposition (*CVD*), are often expensive, technologically complex, and difficult to scale for large-area engineering applications. The present study is focused on the development of a simple, cost-effective, and scalable in-situ spray-coating technique for depositing graphene onto copper substrates using a xylene-based dispersion system. **Materials and methods.** A stable sprayable graphene dispersion was prepared from graphene synthesized using the modified *Hummers* method and dispersed in a mixture of xylene, isopropanol, epoxy binder, and suspension agents. The coating was deposited onto copper substrates under controlled conditions. Structural and surface characterization of the graphene-coated copper substrate was performed using X-ray diffraction (*XRD*), *Raman* spectroscopy, *Fourier*-transform infrared spectroscopy (*FTIR*), and scanning electron microscopy (*SEM*). The graphene layer thickness and interlayer spacing were estimated using *Bragg's* law and the *Scherrer* equation. **Results and Discussion.** *XRD* analysis confirmed the formation of few-layer graphene with an interlayer spacing of 3.37 Å and an estimated thickness corresponding to approximately 5–6 graphene layers. *Raman* spectroscopy revealed the characteristic *D*, *G*, and *2D* bands, confirming successful graphene deposition on the copper substrate. The I_D/I_G ratio decreased from 2.1 for the as-received graphene powder to 0.85 after coating deposition, indicating preferential deposition of better-dispersed graphene sheets. *FTIR* analysis suggested *Cu–O–C* interfacial interactions between graphene and copper. *SEM* observations revealed uniformly distributed wrinkled graphene sheets forming interconnected conductive pathways across the substrate surface. The crystallographic structure of copper remained unchanged after coating, and no secondary phases were detected. ***Conclusions.*** The developed xylene-assisted spray-coating process provides a practical and scalable route for depositing graphene on copper substrates. The resulting coating exhibited an interlayer spacing of 3.37 Å, approximately 5–6 graphene layers, characteristic graphene *Raman* signatures, and a uniform surface morphology. These findings demonstrate the potential of graphene-coated copper substrates for advanced thermal management systems, including condensers, evaporators, phase-change heat exchangers, and high-performance heat-transfer surfaces.

For citation: Giri S.V., Autee A., Kadam A., Shinde R. Structural characterization of graphene-coated copper substrate prepared by scalable In-Situ spray coating using xylene dispersion. *Obrabotka metallov (tekhnologiya, oborudovanie, instrumenty) = Metal Working and Material Science*, 2026, vol. 28, no. 3, pp. 185–204. DOI: 10.17212/1994-6309-2026-28.3-185-204. (In Russian).

Introduction

Efficient energy utilisation in industrial applications depends largely on heat exchange between hot and cold fluids. Heat exchangers are widely employed to enable this process, and improving their thermal efficiency can significantly enhance overall system performance while reducing operational costs. Various approaches have been explored to augment heat transfer, including the use of solid particles with high

*** Corresponding author**
Giri Sudhakar Vitthalrao, Ph.D. (Engineering), Research Scholar
Dr. Babasaheb Ambedkar Marathwada University,
Chhatrapati Sambhajinagar,
431004, Maharashtra, India
Tel.: +91 9850884540, **e-mail:** sudhavgiri@gmail.com

thermal conductivity dispersed in working fluids [1, 2], as well as the application of functional coatings onto heat exchanger surfaces. Among these, graphene-based nanoparticles [3-7] and their coatings on substrates have attracted considerable interest owing to graphene's outstanding intrinsic properties. These characteristics enable the reduction of heat exchanger size while maintaining adequate fluid flow, and make graphene particularly suitable for surface coatings in phase-change heat exchangers, where it can substantially enhance heat transfer rates due to its superior thermal conductivity and hydrophobic properties.

Geim and *Novoselov's* [4] groundbreaking work in 2004 marked the advent of monolayer graphene, distinguished by its exceptional rigidity, electrical and thermal conductivity. The high thermal conductivity of graphene has attracted significant attention in thermal engineering. In this field, researchers have increasingly turned their attention to monolayer graphene instead of traditional materials such as gold, copper, and carbon nanotubes owing to its exceptional thermal conductivity. This makes graphene highly effective for heat dissipation in compact electronic devices. *Balandin* et al. [8] observed that freestanding graphene can surpass the known thermal conductivity of any material, with a value ranging from 2,000 to 4,000 W/mK, which is also much greater than that of diamond. Graphene-coated SiO_2 substrates have shown thermal conductivities of around 600 W/mK, which is approximately 50% higher than that of copper. Additionally, the thermal properties of graphene-related materials have been investigated by simulation [9–11] and experiments [12–14]. *Persson* et al. [15] studied the heat transfer mechanism at the surface contact between graphene layers and SiO_2 substrates, emphasizing the importance of partial surface contact in heat transfer. Their results highlighted the critical role of real contact surfaces in enhancing heat transfer efficiency.

The phase change concept has been adopted in heat transfer technology, having raised great interest in the field, owing to wide industrial applications of such processes. A potential solution to improve the heat transfer performance is to add nanoparticles to the working fluid. *Kim* et al. [16] noted that particles in the fluid could collect on the internal surface wall and form a porous deposit that would raise the surface roughness and hydrophilicity. These changes enhance the evaporation rate and consequently improve overall heat-transfer performance. In a thermosyphon, *Tong* et al. [17] studied and compared the efficiency of the graphene oxide (*GO*) powder loaded working fluid to that of silver oxide (Ag_2O) nanoparticle loaded working fluid. They discovered that even though graphene oxide is hydrophobic, it has excellent permeation efficiency because it arranges in layers with spaces between the layers that allow fluids to penetrate. Further studies by *Ahn* et al. [18, 19] showed that the critical heat flux increased by 70% after using reduced graphene oxide (*RGO*), which is an important boiling heat transfer parameter. This improvement highlights the material's potential in improving the heat transfer performance.

Graphene coatings that promote drop-wise condensation (*DWC*) have attracted attention as they are applied in condensed water vapour systems etc. [20, 21]. In conventional systems, condensation is achieved in film-wise form [21–23] in which a liquid film covers a colder surface, and this mode is preferred by the hydrophobic surfaces of metals that are mostly used in heat exchangers [24]. However, when the wettability of the surface is lowered (e.g. by coating it with a hydrophobic material such as graphene), discrete liquid droplets can develop, grow to the maximum size allowable by gravity and other forces, and then slide along the surface [25]. This promotes dropwise condensation instead of film-wise condensation (*FWC*), which gives substantial benefits. It decreases the resistance to conduction of the fluid film and causes a significant increase in the heat transfer coefficient (*HTC*). The *HTC* is considerably larger for dropwise condensation, typically by an order of magnitude, as compared to *FWC*, particularly in steam condensation. This improvement in *HTC* during *DWC* has profound consequences on the efficiency and performance of a number of industrial condensation processes for more effective heat transfer and energy utilization.

Functionalization of the surface to obtain hydrophobicity is usually necessary to obtain drop-wise condensation (*DWC*) [26, 27]. With its inherent hydrophobic properties, graphene has been established as a potential contender for such coatings. Experimental measurements and simulations have estimated the water contact angle of graphene to be between 95 and 100 degrees [28]. *Rafiee* et al. have also found that graphene films on different substrates are "wetting transparent", and do not change the wettability of the underlying substrate [29]. But as the number of graphene layers increases, this behavior changes

and finally converges to the water contact angle of bulk graphite. In addition, it is possible to improve the hydrophobic properties by nano-structuring the surface of the substrate or by using patterning techniques [30]. This surface modification helps to increase the water contact angle which helps to promote drop-wise condensation. Besides, graphene layers grown on copper substrates have been found to decrease the contact angle hysteresis, which leads to less pinning of water droplets. This property is important to allow the movement of droplets and to maximize the efficiency of the *DWC*.

The uniform graphene coatings are commonly fabricated using chemical vapour deposition (*CVD*) techniques. Alternatively, flakes can be acquired through the exfoliation of graphite and subsequent deposition onto suitable substrates [31, 32]. These methods offer precise control over graphene layer thickness and uniformity, making them advantageous for various applications. However, such processes may be time-consuming, energy-intensive, and cost-prohibitive. Graphene oxide (*GO*) offers several advantages, including good compatibility with organic and aqueous solvents and ease of processability [33]. Through various processes, the wettability of *GO* coatings can be altered to become hydrophobic [34]. While there is a substantial body of literature [28, 35] on the wettability of graphene-based films, studies specifically investigating heat transfer calculations during drop-wise condensation (*DWC*) of vapour remain relatively scarce. However, graphene and graphene oxide have already been explored in pool boiling applications in critical electrical devices [36, 37]. Graphene and *GO* coatings have shown promise in improving heat transfer efficiency in various contexts. For instance, *Rafiee* et al. [29] observed a 30% enhancement in heat transfer on graphene-coated copper substrates compared to bare copper during condensation of humid air. *Haque* et al. [38, 39] investigated the growth of water droplets on *GO*-coated copper substrates and the event of freezing, highlighting the potential applications of graphene-based coatings in managing water-related processes. However, the specific utilisation of graphene-based coatings to enhance heat transfer during steam condensation remains limited.

By using suitable coating methods for graphene over copper and other metallic tubes/substrates combined with various nanofluids, researchers have shown promising improvements in thermal characterization and heat exchange mechanisms. Graphene's remarkable properties and versatility make it a highly sought-after material in various cutting-edge technologies and industrial fields. However, a significant body of reported research has used *GO* solutions, due to which the resulting films often have non-uniform thickness, indicating the need for further exploration of fabrication or coating methods. Due to the limitations of the *CVD* coating method for mass production, selecting other suitable coating methods has remained challenging for the application under consideration. Further investigation of changes in thermal transport properties such as thermal conductivity, diffusivity, and specific heat capacity is needed from a design point of view to extend the application of graphene coating in heat transfer mechanisms. These studies collectively contribute to our understanding of single-droplet evaporation and condensation dynamics, providing insights into the influence of surface properties and morphology on phase change heat transfer processes.

The modified *Hummers* method is a well-acknowledged and accepted method for chemical exfoliation of graphene and its derivatives [40]. This method yields *GO*, which, after reduction, gives *RGO*. Further reduction and chemical treatment yield graphene in single or few layers, depending on the degree of reduction. However, graphene obtained by the modified *Hummers* method contains various defects and functional groups at different locations. Though it yields defective graphene, it can be considered a superior method for producing a large quantity of graphene and its derivatives directly from graphite.

Three isomers of dimethyl benzene are grouped together as xylene. Ethylbenzene and xylene isomers are important in the petrochemical industry as a basis for the synthesis of many organic compounds [41]. Xylene's structure is a benzene ring with two methyl (CH_3) groups, leading to three isomers: ortho-, meta-, and para-xylene. These isomers have the same chemical formula C_8H_{10} or $C_6H_4(CH_3)_2$ but differ in the positions of the methyl groups on the ring [42]. Though graphene has inherently excellent physical properties, its anisotropic nature has raised many challenges in harnessing them for practical applications. Graphene or its derivative's coating on a suitable substrate is one of the methods considered to harness these excellent properties. While most applications do not employ graphene dispersions directly, many of them require graphene to be dispersed at some point during the process (e.g. the deposition of thin films

of graphene), therefore, the stability, concentration, and overall quality of the dispersion remain extremely important [43].

Various methods with different solvents are used for the preparation of graphene dispersions for different applications. Physical dispersion method is advantageous over chemical oxidative grafting to protect and preserve the excellent properties of graphene [44]. In physical dispersion method**,** graphene-polymer binding is possible through two weak bonding forces: *C–H…*$\boldsymbol{\pi}$ and $\boldsymbol{\pi}$–$\boldsymbol{\pi}$; however, $\boldsymbol{\pi}$–$\boldsymbol{\pi}$ bonding allows for a tighter adsorption bond between graphene and the polymer [45–48]. The intercalation of polymer solvent between graphene layers through these weak bonding forces may form steric hindrance through $\boldsymbol{\pi}$–$\boldsymbol{\pi}$ adsorption to disperse graphene; however, to bind graphene to a polymer via $\boldsymbol{\pi}$–$\boldsymbol{\pi}$ bonding, the polymer is also required to have a hexatomic ring structure [49]. *Liu* et al. [49] first reported a xylene-based dispersion of graphene in aromatic petroleum resin by solution mixing and studied the effect of xylene content on dispersion quality. The obtained graphene dispersion solution was then used to coat 2024 aluminum alloy plates to investigate their corrosion protection performance. This study was accompanied by various characterization techniques such as *XRD*, *Raman* spectroscopy**,** and *SEM* to confirm the presence of graphene in the applied coatings on aluminum alloy substrates. Their study confirmed successful dispersion of graphene in aromatic petroleum resins (*APR*) for corrosion protection performance; however, hydrophobic characterization was not focused. Despite the promising results reported for graphene dispersion in xylene-based systems, there remains limited understanding of scalable spray-deposition approaches for producing graphene coatings on copper substrates intended for thermal-management applications. Most reported studies have focused either on corrosion protection or graphene oxide-based coatings, while investigations addressing direct graphene deposition, structural characterization, and coating–substrate interactions through a simple and industrially scalable spray process remain scarce. This research gap motivated the present investigation.

Graphene with epoxy binders for coatings has been reported in some available literature. However, when hardener is added, the agglomeration of graphene in the base solvent with resin is one of the major hurdles in preparing a sustainable spray solution for metal substrates for mechanical applications. The spray coating method, which is ideal for a uniform thin coating, requires a comparatively thinner spray solution than other methods.

The purpose of the present study is to develop a scalable xylene-assisted spray-coating process for the deposition of graphene onto copper substrates and to investigate the structural characteristics of the resulting graphene-coated copper system.

To achieve this purpose, ***the following objectives*** were established:

– to prepare a stable graphene dispersion using a xylene-based solvent system;
– to deposit graphene on copper substrates through an in-situ spray-coating process;
– to investigate the crystallographic characteristics of graphene using *XRD* analysis;
– to evaluate structural defects and layer characteristics using *Raman* spectroscopy;
– to investigate interfacial interactions between graphene and copper using *FTIR*;
– to examine coating morphology using *SEM*;
– to assess the suitability of the developed coating process for thermal-management applications.

Materials and methods

Materials

Commercial graphene powder synthesized via an enhanced oxidative exfoliation (modified *Hummers* method) and procured from *KNV Incorporation*, *Nagpur*, India, was utilized in this investigation. The modified *Hummers* method is widely recognized as an efficient and scalable route for the production of graphene-based materials, although it may introduce structural defects and residual oxygen-containing functional groups during the oxidation and exfoliation processes. Prior to coating preparation, the as-received graphene powder was comprehensively characterized using X-ray diffraction (*XRD*), Raman spectroscopy, *Fourier* transform infrared spectroscopy (*FTIR*), and scanning electron microscopy (*SEM*).

XRD analysis confirmed the graphitic structure with an interlayer spacing of 3.37 Å and an estimated graphene stack thickness corresponding to approximately 5–6 graphene layers. *Raman* spectroscopy exhibited the characteristic *D*, *G*, and *2D* bands of graphene with an I_D/I_G ratio of 2.1, indicating the presence of structural defects typically associated with chemically exfoliated graphene. *SEM* observations revealed the characteristic wrinkled and layered morphology of exfoliated graphene sheets. These characterization results confirmed the suitability of the graphene powder for preparing stable dispersions and subsequent spray-coating applications.

The selection of graphene synthesized by the modified *Hummers* method was based on its scalability, commercial availability, and suitability for large-area coating applications. Although alternative synthesis methods such as chemical vapour deposition can produce higher-quality graphene with fewer defects, they are generally associated with higher processing costs and lower production scalability. Therefore, chemically exfoliated graphene was considered more appropriate for the present investigation, which focuses on the development of a practical and scalable spray-coating process.

Methods of Characterization Techniques

The structural, morphological, and chemical characteristics of the graphene powder and graphene-coated copper substrates were investigated using a combination of X-ray diffraction (*XRD*), Raman spectroscopy, *Fourier* transform infrared spectroscopy (*FTIR*), and field emission scanning electron microscopy (*FESEM*). The characterization techniques and operating parameters employed in the present study are summarized in Table 1.

Table 1

Characterization techniques, instrumentation, operating parameters, and purpose of analysis used in the present study

Technique	Instrument	Operating Parameters	Purpose
XRD	*Bruker D8 Advance*	*Cu-K*α, λ = 1.5406 Å	Crystal structure and layer estimation
Raman	*Horiba Xplora Plus*	**5**32 nm laser, 1,200 grooves mm^{-1}	Defect density and layer characterization
FTIR	*Shimadzu FTIR*	400–4,000 cm^{-1}	Functional group analysis
FE-SEM	*JEOL FESEM*	Appropriate accelerating voltage	Surface morphology analysis
*EDS**	*Oxford Inca*	Coupled with *FESEM*	Elemental analysis

The crystal structure, phase composition, and interlayer spacing of graphene and graphene-coated copper specimens were analyzed using X-ray diffraction (*Bruker D8 Advance*, Germany) with *Cu-K***α** radiation (**λ** = 1.5406 Å) over the selected diffraction range. The crystallite thickness and estimated graphene layer number were calculated using the *Scherrer* equation and *Bragg's* law.

Raman spectroscopy (*Xplora Plus*, *Horiba Scientific*, France) equipped with a 532 nm excitation laser and a 1,200 grooves mm^{-1} diffraction grating was used to evaluate the structural quality, defect density, and layer characteristics of graphene. The laser power was carefully controlled to prevent local thermal damage to the deposited graphene. To obtain improved spectral resolution and assess coating uniformity, additional graphene films were prepared on glass substrates using drop-casting and spin-assisted spreading techniques.

The functional groups and interfacial chemical interactions between graphene and copper were examined using *Fourier* transform infrared spectroscopy (*FTIR*, *Shimadzu*, Japan) in the spectral range of 400–4,000 cm^{-1}.

Surface morphology was examined using field emission scanning electron microscopy **(***FESEM*, *JEOL*, Japan**)**. Prior to *FESEM* examination, the samples were coated with a thin conductive layer to minimize charging effects and improve image quality. *SEM* imaging was performed at appropriate accelerating voltages and working distances to observe graphene sheet morphology, surface coverage, and coating uniformity. Energy-dispersive X-ray spectroscopy (*EDS*) was employed in conjunction with *FESEM* to determine the

elemental composition of the coated surfaces and to verify the presence of carbon-rich graphene deposits on the copper substrate.

The average coating thickness was measured at multiple locations using microscopic image analysis, and the mean value was reported to assess coating uniformity and deposition consistency.

Results and discussion

The X-ray diffraction (XRD) analysis

XRD analysis was performed to investigate the structural properties of the synthesized graphene powder and the spray-coated film on the copper substrate. As presented in Fig. 1, the *XRD* pattern of the graphene powder exhibits a broad diffraction peak centered at approximately $2\theta \approx 26°$, corresponding to the (002) plane of graphitic carbon, which agrees well with the standard *ICSD* card No. 00-001-0640. The broad nature of this peak indicates the presence of few-layer graphene with partial disorder in the stacking of graphene sheets, suggesting a turbostratic structure [50, 51]. Such broad reflections are generally attributed to the reduced crystalline order along the c-axis and the nanoscale thickness of exfoliated graphene sheets [52]. The absence of additional peaks in the *XRD* profile confirms the high phase purity of the synthesized graphene and indicates that no significant crystalline impurities such as graphite oxide or amorphous carbon are present [53].

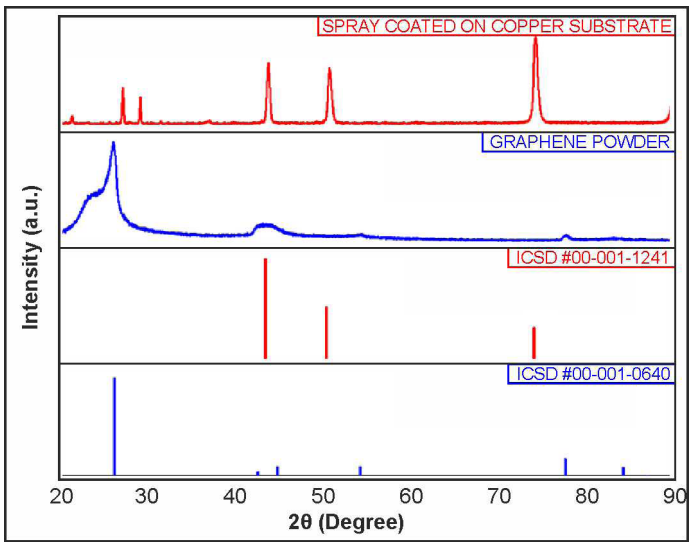

Fig. 1. XRD patterns of the graphene powder and the spray-coated film on the copper substrate, shown with the standard *ICSD* reference pattern

XRD analysis was also used to estimate the number of graphene layers using *Bragg's* law and the *Scherrer* equation. The obtained *XRD* data were fitted with a non-linear *Gaussian* function, yielding a full width at half maximum (*FWHM*) of 4.43° at a peak position of $2\theta = 25.3°$. The (002) reflection at $2\theta = 26.4°$ was used to calculate the interplanar spacing $d = 3.37$ Å. The *Scherrer* equation was then applied to determine the crystallite thickness (Lc) = 1.84 nm, using a *Scherrer* constant $K = 0.9$, which is commonly used for graphitic carbon materials. From *Gaussian* fitting, the *FWHM* was 4.43 ± 0.10°, the interlayer spacing was 3.37 ± 0.02 Å, and the crystallite thickness was 1.84 ± 0.08 nm.

The estimated layer number obtained from *XRD* analysis represents an average crystallographic thickness of the graphene stacks and should therefore be interpreted as a bulk structural parameter. The number of layers N was calculated using $N = Lc/d$, where d is the interplanar spacing and Lc is the crystallite stack thickness.

Although *Raman* spectroscopy of the coated film exhibited a relatively low I_{2D}/I_G ratio (~0.1), suggesting multilayer graphene behavior, this does not necessarily contradict the *XRD*-derived layer estimate. *Raman*

spectroscopy probes localized surface regions, whereas *XRD* provides an average structural assessment over a larger volume. Therefore, local agglomeration and non-uniform stacking of graphene sheets during spray deposition may result in *Raman* signatures characteristic of thicker multilayer regions while maintaining an average crystallite thickness corresponding to approximately 5–6 graphene layers.

The *XRD* pattern of the spray-coated graphene film on the copper substrate exhibits three dominant and sharp peaks at $2\theta = 43.3°$, 50.4°, and 74.1°, corresponding to the (111), (200), and (220) planes of face-centered cubic (*FCC*) copper, in agreement with *ICSD* card no. 00-001-1241. These sharp and intense peaks confirm the high crystallinity and metallic nature of the copper substrate [54].

However, the extremely thin nature of the deposited graphene layer, combined with the significantly higher scattering intensity of the copper substrate, limits the detectability of the graphene (002) reflection in conventional θ–2θ *XRD* measurements. Grazing-incidence X-ray diffraction (*GIXRD*) could provide improved surface sensitivity and facilitate more direct observation of the graphene diffraction peak. Nevertheless, the present study relied on complementary *Raman* spectroscopy and *FTIR* analyses to confirm the successful deposition of graphene on the copper substrate**,** which masks the weak signal arising from the thin graphene layer [55]. Furthermore, because the carbon atomic scattering factor is smaller than that of copper, the graphene peak is not as visible as it would be in the diffraction pattern of copper. There are no extra diffraction peaks or shifts, which means that the crystal structure of the copper substrate remains unchanged during the spray-coating process. This implies that the deposition process does not damage the substrate, which agrees with previously reported results for graphene or carbon coatings on metal substrates in solution-based or thermal deposition.

In summary, the *XRD* results confirm the presence of few-layer graphitic structures in the synthesized graphene powder and demonstrate that the spray-coating process successfully deposited graphene onto the copper substrate without inducing detectable structural changes, secondary phases, or crystallographic distortion in the underlying copper substrate.

Spectroscopic analysis

FTIR analysis

FTIR spectra of *Cu*, *Gr*, and *Gr@Cu* samples are shown in Fig. 2 and provide information on the functional groups, interfacial interactions, and chemical bonding associated with the deposited graphene coating.

For the bare copper substrate, two absorption bands were observed at approximately 1,540 cm^{-1} and 3,355 cm^{-1}. The broad band centered at 3,355 cm^{-1} is assigned to *O–H* stretching vibrations from surface hydroxyl species and adsorbed moisture due to atmospheric exposure. The feature at 1,540 cm^{-1} is attributed

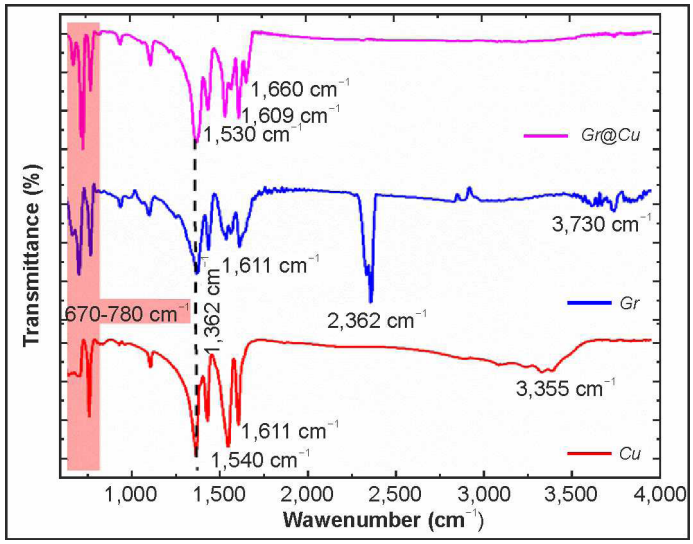

Fig. 2. FTIR spectra of the *Cu*, *Gr*, and *Gr@Cu* samples

to surface-associated oxygen-containing species and adsorbed molecular groups, rather than to direct *Cu–O* stretching vibrations, which are typically reported below 700 cm^{-1}, and the bending vibrations of adsorbed water, respectively.

The presence of a thin native oxide layer on the copper surface resulting from atmospheric exposure is reflected by the broad band at 3,355 cm^{-1}, assigned to *O–H* stretching of surface hydroxyl species.

For the graphene (*Gr*) sample, the characteristic peaks are observed at 1,362 cm^{-1} (*C–O* stretching, epoxy or hydroxyl) and 1,611 cm^{-1} (*C=C* stretching of sp^2-hybridised carbon atoms).

A weak feature near 2,362 cm^{-1} is also detected; however, this band is most likely an instrumental artefact from atmospheric CO_2 in the *FTIR* optical path. The broad band near 3,730 cm^{-1} is attributed to residual hydroxyl groups. Overall, these spectral features indicate the presence of few-layer graphene with limited oxygen-containing functionalities, which is typical of chemically exfoliated graphene prepared via the modified *Hummers* method.

The *Gr@Cu* composite shows new peaks at 1,530; 1,609; and 1,660 cm^{-1}, assigned to *C–C* and *C=O* stretching vibrations of graphitic and carboxylic domains, respectively. Additional low-wavenumber bands in the range 670–780 cm −1 are assigned to *Cu–O–C* and/or *Cu–O* bonds, indicating interfacial chemical bonding between graphene and the copper substrate. The broad *O–H* band observed in bare *Cu* is diminished or absent, suggesting that the surface is fully covered and protected from further oxidation. The 1,610 cm^{-1} band of *Cu* and *Gr@Cu* overlap, indicating strong chemical coupling between the two phases.

The appearance of *Cu–O–C* stretching bands in the 670–780 cm^{-1} range and the reduction in oxygen-containing groups relative to *Gr* indicate successful interfacial interaction during coating and partial reduction of graphene. The spectral changes observed for *Gr@Cu* confirm successful graphene deposition and the formation of strong interfacial interactions. The bands in the 670–780 cm^{-1} region suggest the formation of *Cu–O–C* interfacial linkages, while the decrease in oxygen-containing functional groups relative to the graphene powder indicates partial reduction and stabilization of the deposited graphene layer. These observations indicate a chemically stable and continuous graphene coating on the copper surface.

Such interfacial interactions are expected to improve coating stability and facilitate energy transfer across the graphene–copper interface, which is beneficial for thermal management applications. However, direct thermal conductivity measurements were beyond the scope of the present study and will be addressed in future work.

Efficient phonon transport across the *Gr–Cu* interface is achieved by reducing interfacial thermal resistance, which is supported by *Cu–O–C* linkages and enhanced graphitic bonding. This improved phonon–electron coupling enhances heat conduction and also provides protection against oxidation and corrosion. Overall, *FTIR* confirms the successful formation of a chemically bonded *Gr@Cu* hybrid structure with structural and thermal advantages for efficient and durable heat exchanger applications. The bonding and stretching assignments for *Cu*, *Gr*, and *Gr@Cu* samples are summarized in Tables 2–4.

Raman spectroscopic analysis

Raman spectroscopy is a non-destructive, versatile, and widely used characterization technique for carbon-based materials [56]. It is commonly employed together with other methods, to identify carbon

Table 2

***FTIR* band assignment for *Cu* sample**

Wavenumber (cm^{-1})	Vibration / Functional group	Assigned bond / Mode	Interpretation
1,540	Surface-associated oxygen species	Adsorbed oxygen-containing groups	Indicates surface oxidation products and adsorbed molecular species
1,611	*H–O–H* bending vibration	Adsorbed moisture	Surface moisture from atmospheric exposure
3,355	*O–H* stretching	Hydroxyl groups	Presence of surface hydroxyl species and adsorbed water molecules

Table 3

***FTIR* band assignment for graphene (*Gr*) sample**

Wavenumber (cm^{-1})	Vibration / Functional group	Assigned bond / Mode	Interpretation
1,362	*C–O* stretching	Residual oxygen-containing groups	Indicates incomplete removal of oxygen functionalities
1,611	*C=C* stretching	Graphitic backbone vibration	Confirms the graphitic carbon network
2,362	Atmospheric CO_2	Instrumental artefact	Associated with CO_2 in *FTIR* optical path
3,730	*O–H* stretching	Residual hydroxyl groups	Evidence of remaining oxygen-containing species

Table 4

***FTIR* band assignment for graphene-coated copper (*Gr@Cu*)**

Wavenumber (cm^{-1})	Vibration / Functional group	Assigned bond / Mode	Interpretation
1,530	*C=C* stretching	Graphitic domain vibration	Confirms graphene layer on the *Cu* surface
1,609	*C=C* stretching / *Cu–O* overlap	**π**-bond stretching	Indicates strong interfacial coupling between *Cu* and graphene
1,660	*C=O* stretching	Carbonyl / carboxylic groups	Suggests partial oxidation or interfacial functionalization
670–780	*Cu–O–C* / *Cu–O* stretching	Interfacial bonding mode	Evidence of *Cu–O–C* linkage between the metal and graphene layers

allotropes and enables both quantitative and qualitative analysis of graphitic carbon materials. The distinct *D*, *G*, and *2D* band positions are characteristic of graphite, graphene oxide (*GO*), reduced graphene oxide (*RGO*), and graphene. Graphene is characterized by the presence of three distinct bands: the *D* band around 1,350 cm^{-1} is attributed to defects; the *G* band between 1,550 and 1,600 cm^{-1} corresponds to the in-plane stretching vibration of sp^2-hybridised carbon atoms in the honeycomb lattice; and the *2D* band, which is an overtone of the *D* band at 2,650–2,750 cm^{-1}, is considered a characteristic feature of graphene.

Depending on the reduction degree and synthesis route, the *D* band may be present or absent, but the *2D* band together with the G band are essential to confirm graphene on a substrate [56]. Defect-free single-layer graphene (*SLG*) exhibits a sharp, intense *2D* peak around 2,700 cm^{-1} relative to the other bands (Fig. 3). The *2D* band intensity decreases with increasing layer number. Although less intense, the presence of the *2D* band indicates graphene even in multilayer samples.

The graphene powder used in this study was prepared via the modified *Hummers* method followed by reduction. In *Raman* spectroscopic analysis, all three aforementioned bands appear at their characteristic positions. As shown in Fig. 4, the *D*, *G*, and *2D* bands are observed at 1,310 cm^{-1}, 1,596 cm^{-1}, and 2,675 cm^{-1}, respectively. The $\boldsymbol{I_D/I_G}$ ratio is 2.1, while the $\boldsymbol{I_{2D}/I_G}$ ratio is 0.25, indicating that the sample consists of few-layer graphene, which is consistent with the *XRD* results. The number of layers calculated from the (002) peak at $2\boldsymbol{\theta} \approx 26°$ was estimated as 5–6, which is in good agreement with reported literature.

The same graphene powder was used to prepare the xylene-based graphene spray solution. As shown in Fig. 4, the *Raman* spectrum of the spray coating on the copper substrate indicates that graphene was well dispersed in the spray solution and deposited uniformly on the substrate. All characteristic bands of graphene appear at their expected wavenumber positions. In Fig. 4, the *D*, *G*, and *2D* bands are observed at 1,357 cm^{-1}; 1,593 cm^{-1}; and 2,670 cm^{-1}, respectively. The $\boldsymbol{I_D/I_G}$ ratio is 0.85, while the $\boldsymbol{I_{2D}/I_G}$ ratio is 0.1, indicating a reduction in defect density.

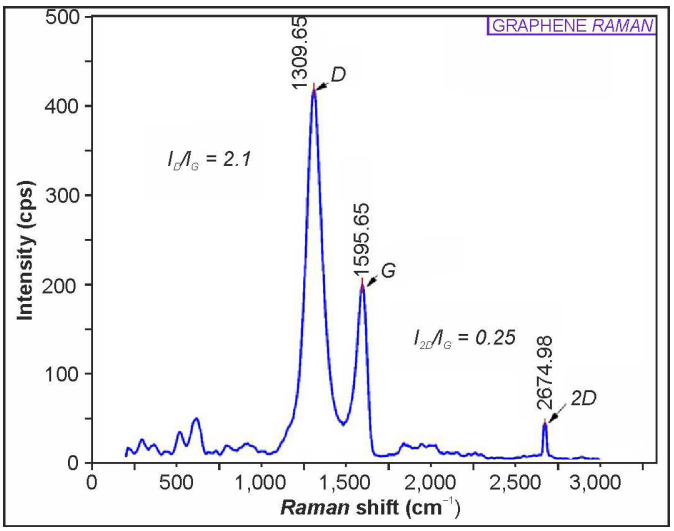

Fig. 3. Raman spectroscopy of graphene powder obtained by making a thin film on glass substrates

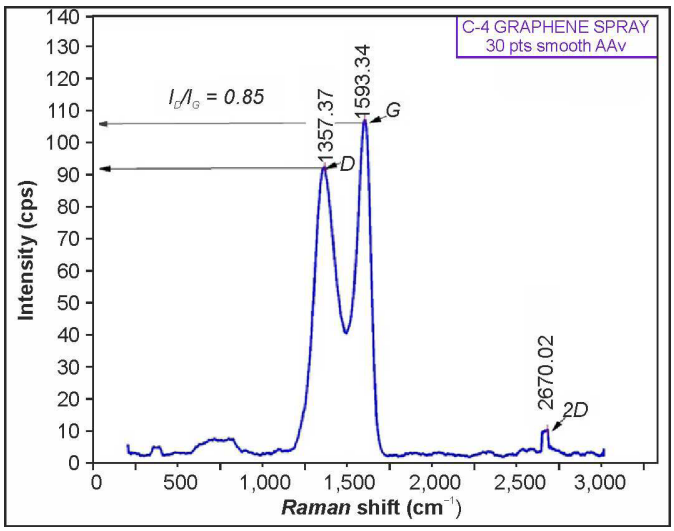

Fig. 4. Raman spectrum of the xylene-based graphene spray coating on the copper substrate

The decrease in the $\boldsymbol{I_D/I_G}$ ratio from 2.1 to 0.85 should not be interpreted as structural healing of graphene by xylene. Rather, the reduction is likely associated with preferential dispersion and deposition of less-defective graphene sheets during spray coating, while highly defective agglomerates remain sedimented during dispersion preparation. This is supported by the comparatively less intense *D* peak relative to the *G* peak. These observations indicate that xylene can be used as an effective dispersing agent for preparing a stable, sprayable graphene suspension. This finding could facilitate large-scale graphene coating processes on heat exchanger materials for efficient and effective energy management.

Although *XRD* analysis indicates approximately 5–6 graphene layers, the low $\boldsymbol{I_{2D}/I_G}$ ratio (~0.1) observed in *Raman* spectroscopy suggests multilayer graphene behavior. This apparent discrepancy may arise from local agglomeration and non-uniform stacking of graphene sheets during spray deposition. While *XRD* provides an average bulk structural assessment, *Raman* spectroscopy probes localized surface regions. Therefore, thicker graphene agglomerates at specific locations may contribute to the observed *Raman* response.

Morphological characterization

SEM analysis

The *SEM* micrographs in Fig. 5 provide a detailed view of the surface morphology and microstructural features of the investigated samples. Images (*a*) and (*b*) show the *Gr@Cu* hybrid, in which graphene sheets are uniformly distributed and appear compact with some agglomeration on the copper substrate. The graphene layers exhibit typical wrinkling and folding, forming interconnected networks capable of bridging gaps between the copper grains.

Both features enhance thermal transfer and electron conduction in heat exchanger systems, as the conformal coating creates continuous conductive pathways. The observed agglomerated morphology suggests a strong interfacial bond between copper and graphene, resulting in improved mechanical integrity and reduced interfacial thermal resistance.

In contrast, images (*c*) and (*d*) show the bare copper surface with a smoother, grain-like morphology, metallic lustre, and well-defined grain boundaries. The copper surface is compact but lacks the interconnected nanosheet network observed in the hybrid sample. Without graphene coverage, phonon coupling is reduced and interfacial scattering is increased, leading to lower thermal transfer efficiency compared with *Gr@Cu*.

The morphology of the graphene powder prepared via the modified *Hummers* method is shown in images (*e*) and (*f*) and exhibits thin, wrinkled, and layered sheets characteristic of exfoliated graphene, often

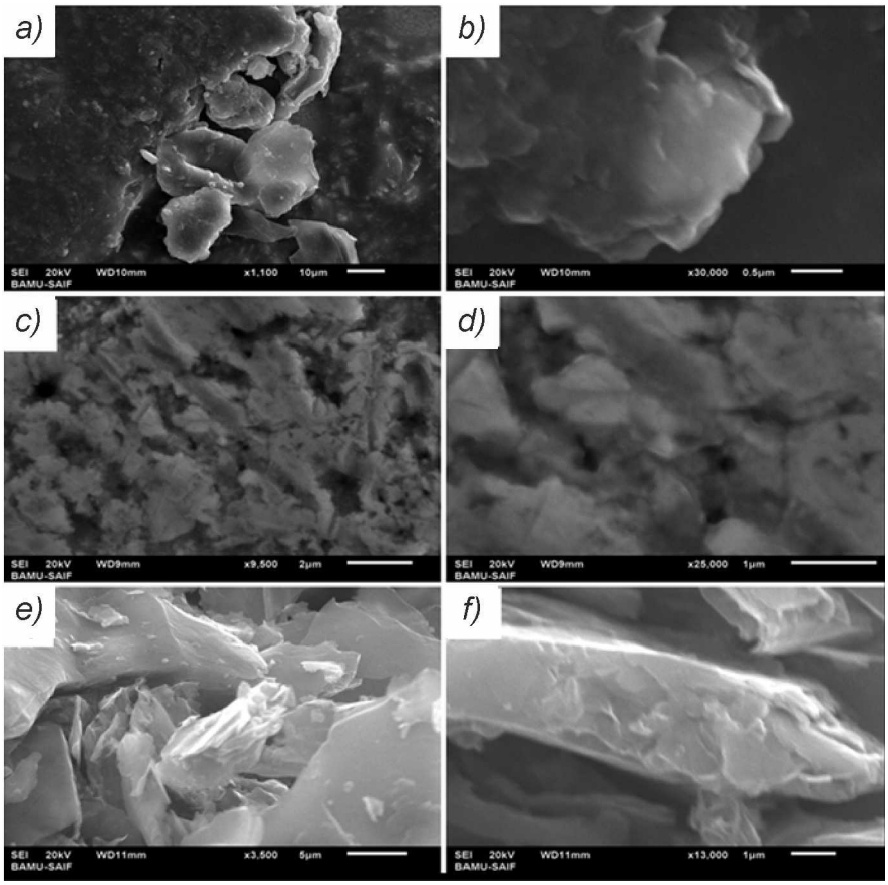

Fig. 5. *SEM* images of (*a*, *b*) *Gr@Cu*, (*c*, *d*) the *Cu* substrate, and (*e*, *f*) the *Gr* sample

in stacked or partially crumpled form. This morphology provides a high surface area and intrinsic thermal conductivity, further supporting the suitability of graphene as a coating for metallic substrates.

Overall, the continuous yet agglomerated nature of *Gr@Cu* suggests potential for advanced heat exchange and thermal management applications, providing a promising direction for further development.

SEM imaging was performed at an accelerating voltage of 15 kV and a working distance of approximately 10 mm. Scale bars are included in all micrographs.

Conclusion

1. **A** scalable xylene-assisted spray-coating process was successfully developed for graphene deposition on copper substrates.

2. *XRD* analysis confirmed few-layer graphene with an interlayer spacing of 3.37 ± 0.02 Å and approximately 5–6 graphene layers.

3. *Raman* spectroscopy revealed characteristic *D*, *G*, and *2D* bands with a decrease in the $\boldsymbol{I_D/I_G}$ ratio from 2.1 to 0.85 after coating deposition.

4. *FTIR* analysis confirmed interfacial interactions between graphene and copper via *Cu–O–C* bonding features.

5. *SEM* analysis showed interconnected wrinkled graphene networks distributed over the copper substrate surface.

6. The developed coating system shows potential for thermal-management applications, including evaporators, condensers, and phase-change heat exchangers.

7. Future work will focus on coating thickness optimization, adhesion testing, contact-angle measurement, and thermal conductivity evaluation.

References

1. Marzouk S.A., Abou Al-Sood M.M., El-Said E.M.S., Younes M.M., El-Fakharany M.K. A comprehensive review of methods of heat transfer enhancement in shell and tube heat exchangers. *Journal of Thermal Analysis and Calorimetry*, 2023, vol. 148, pp. 7539–7578.

2. Pungaiya S., Kailasanathan C. A review of surface coating technology to increase the heat transfer. *International Journal of Mechanical Engineering and Robotics Research*, 2018, vol. 7 (5), pp. 458–465.

3. Liu C., Chen M., Yu W., He Y. Recent advance on graphene in heat transfer enhancement of composites. *ES Energy & Environment*, 2018, vol. 2, pp. 31–42. Available at: http://www.espublisher.com/journals/articledetails/72/ (accessed 11.08.2026).

4. Novoselov K.S., Geim A.K., Morozov S.V., Jiang D., Zhang Y., Dubonos S.V., Grigorieva I.V., Firsov A.A. Electric field effect in atomically thin carbon films. *Science*, 2004, vol. 306 (5696), pp. 666–669.

5. Balandin A.A., Ghosh S., Bao W., Calizo I., Teweldebrhan D., Miao F., Lau C.N. Superior thermal conductivity of single-layer graphene. *Nano Letters*, 2008, vol. 8 (3), pp. 902–907.

6. Ma L., Wang Y., Xu X., Wang Y., Wang C. Structural evolution and thermal conductivity of flexible graphite films prepared by carboxylic graphene/polyimide. *Ceramics International*, 2021, vol. 47 (1), pp. 1076–1085.

7. Wang K., Li M., Zhang J., Lu H. Polyacrylonitrile coupled graphite oxide film with improved heat dissipation ability. *Carbon*, 2019, vol. 144, pp. 249–258.

8. Ghosh S., Bao W., Nika D.L., Subrina S., Pokatilov E.P., Lau C.N., Balandin A.A. Dimensional crossover of thermal transport in few-layer graphene. *Nature Materials*, 2010, vol. 9 (7), pp. 555–558.

9. Ma D., Ding H., Wang X., Yang N., Zhang X. The unexpected thermal conductivity from graphene disk, carbon nanocone to carbon nanotube. *International Journal of Heat and Mass Transfer*, 2017, vol. 108, pp. 940–944.

10. Ghasemi H., Rajabpour A., Akbarzadeh A.H. Tuning thermal conductivity of porous graphene by pore topology engineering: Comparison of non-equilibrium molecular dynamics and finite element study. *International Journal of Heat and Mass Transfer*, 2018, vol. 123, pp. 261–271.

11. Subrina S., Kotchetkov D., Balandin A.A. Heat removal in silicon-on-insulator integrated circuits with graphene lateral heat spreaders. *IEEE Electron Device Letters*, 2009, vol. 30 (12), pp. 1281–1283.

12. Yan Z., Liu G., Khan J.M., Balandin A.A. Graphene quilts for thermal management of high-power GaN transistors. *Nature Communications*, 2012, vol. 3, p. 827.

13. Malekpour H., Chang K.H., Chen J.C., Lu C.Y., Nika D.L., Novoselov K.S., Balandin A.A. Thermal conductivity of graphene laminate. *Nano Letters*, 2014, vol. 14 (9), pp. 5155–5161.

14. Shahil K.M.F., Balandin A.A. Thermal properties of graphene and multilayer graphene: Applications in thermal interface materials. *Solid State Communications*, 2012, vol. 152 (15), pp. 1331–1340.

15. Persson B.N.J., Ueba H. Heat transfer between graphene and amorphous SiO_2. *Journal of Physics: Condensed Matter*, 2010, vol. 22 (46). DOI: 10.1088/0953-8984/22/46/462201.

16. Kim S.J., Bang I.C., Buongiorno J., Hu L.W. Effects of nanoparticle deposition on surface wettability influencing boiling heat transfer in nanofluids. *Applied Physics Letters*, 2006, vol. 89 (15).

17. Li Tong W., Ong W.J., Chai S.P., Tan M.K., Mun Hung Y. Enhanced evaporation strength through fast water permeation in graphene-oxide deposition. *Scientific Reports*, 2015, vol. 5 (1).

18. Ahn H.S., Kim J.M., Park C., Jang J.-W., Lee J.S., Kim H., Kaviany M., Kim M.H. A novel role of three-dimensional graphene foam to prevent heater failure during boiling. *Scientific Reports*, 2013, vol. 3, p. 1960.

19. Ahn H.S., Kim J.M., Kim J.M., Park S.C., Hwang K., Jo H.J., Kim T., Jerng D.W., Kaviany M., Kim M.H. Boiling characteristics on the reduced graphene oxide films. *Experimental Thermal and Fluid Science*, 2015, vol. 60, pp. 361–366.

20. Chang H., Wu H. Graphene-based nanomaterials: Synthesis, properties, and optical and optoelectronic applications. *Advanced Functional Materials*, 2013, vol. 23 (16), pp. 1984–1997.

21. Yu X., Cheng H., Zhang M., Zhao Y., Qu L., Shi G. Graphene-based smart materials. *Nature Reviews Materials*, 2017, vol. 2 (9), p. 17046.

22. Sun Z., Chang H. Graphene and graphene-like two-dimensional materials in photodetection: Mechanisms and methodology. *ACS Nano*, 2014, vol. 8 (5), pp. 4133–4156.

23. Renteria J.D., Nika D.L., Balandin A.A. Graphene thermal properties: Applications in thermal management and energy storage. *Applied Sciences*, 2014, vol. 4, pp. 525–547.

24. Schrader M.E. Wettability of clean metal surfaces. *Journal of Colloid and Interface Science*, 1984, vol. 100 (2), pp. 372–380.

25. Sikarwar B.S., Khandekar S., Agrawal S., Kumar S., Muralidhar K. Dropwise condensation studies on multiple scales. *Heat Transfer Engineering*, 2012, vol. 33 (4–5), pp. 301–341.

26. Paxson A.T., Yagüe J.L., Gleason K.K., Varanasi K.K. Stable dropwise condensation for enhancing heat transfer via the initiated chemical vapor deposition (iCVD) of grafted polymer films. *Advanced Materials*, 2014, vol. 26, pp. 418–423.

27. Parin R., Del Col D., Bortolin S., Martucci A. Dropwise condensation over superhydrophobic aluminium surfaces. *Journal of Physics: Conference Series*, 2016, vol. 745, p. 032134.

28. Raj R., Maroo S.C., Wang E.N. Wettability of graphene. *Nano Letters*, 2013, vol. 13, pp. 1509–1515.

29. Rafiee J., Mi X., Gullapalli H., Thomas A.V., Yavari F., Shi Y., Ajayan P.M., Koratkar N.A. Wetting transparency of graphene. *Nature Materials*, 2012, vol. 11, pp. 217–222.

30. Singh E., Thomas A.V., Mukherjee R., Mi X., Houshmand F., Peles Y., Peles Y., Shi Y., Koratkar N.. Graphene drape minimizes the pinning and hysteresis of water drops on nanotextured rough surfaces. *ACS Nano*, 2013, vol. 7 (4), pp. 3512–3521.

31. Thema F.T., Moloto M.J., Dikio E.D., Nyangiwe N.N., Kotsedi L., Maaza M., Khenfouch M. Synthesis and characterization of graphene thin films by chemical reduction of exfoliated and intercalated graphite oxide. *Journal of Chemistry*, 2013, vol. 1, p. 150536.

32. Edwards R.S., Coleman K.S. Graphene synthesis: Relationship to applications. *Nanoscale*, 2013, vol. 5, pp. 38–51.

33. Zhu Y., Murali S., Cai W., Li X., Suk J.W., Potts J.R., Ruoff R.S. Graphene and graphene oxide: Synthesis, properties, and applications. *Advanced Materials*, 2010, vol. 22, pp. 3906–3924.

34. Perrozzi F., Prezioso S., Ottaviano L. Graphene oxide: From fundamentals to applications. *Journal of Physics: Condensed Matter*, 2015, vol. 27.

35. Zhang X., Wan S., Pu J., Wang L., Liu X. Highly hydrophobic and adhesive performance of graphene films. *Journal of Materials Chemistry*, 2011, vol. 21, pp. 12251–12258.

36. Jaikumar A., Kandlikar S.G., Gupta A. Pool boiling enhancement through graphene and graphene oxide coatings. *Heat Transfer Engineering*, 2017, vol. 38, pp. 1274–1284.

37. Gupta A., Jaikumar A., Kandlikar S.G., Rishi A., Layman A. A multiscale morphological insight into graphene-based coatings for pool boiling applications. *Heat Transfer Engineering*, 2018, vol. 39, pp. 1331–1342.

38. Haque M.R., Betz A.R. Frost formation on aluminum and hydrophobic surfaces. *Proceedings of the ASME 16th International Conference on Nanochannels, Microchannels, and Minichannels*, 2018. DOI: 10.1115/ICNMM2018-7609.

39. Haque M.R., Das S.R., Betz A.R. Experimental investigation of condensation and freezing phenomena on hydrophilic and hydrophobic graphene coating. *Applied Thermal Engineering*, 2019, vol. 160, p. 113987.

40. Hidayah N.M.S., Liu W.W., Lai C.W., Noriman N.Z., Khe C.S., Hashim U., Lee H.C. Comparison on graphite, graphene oxide and reduced graphene oxide: Synthesis and characterization. In: *AIP Conference Proceedings*, 2017, vol. 1892. DOI: 10.1063/1.5005764.

41. Rodrigues W.L., Mattedi S., Abreu J.C.N. Vapor-liquid equilibria data for binary systems of ethylbenzene + xylene isomers at 100.65 kPa. *Journal of Chemical and Engineering Data*, 2005, vol. 50 (4), pp. 1134–1138.

42. Zhou Y., Wu J., Lemmon E.W. Thermodynamic properties of o-xylene, m-xylene, p-xylene, and ethylbenzene. *Journal of Physical and Chemical Reference Data*, 2012, vol. 41 (2).

43. Johnson D.W., Dobson B.P., Coleman K.S. A manufacturing perspective on graphene dispersions. *Current Opinion in Colloid and Interface Science*, 2015, vol. 20, pp. 367–382.

44. Parviz D., Das S., Ahmed H.S.T., Irin F., Bhattacharia S., Green M.J. Dispersions of non-covalently functionalized graphene with minimal stabilizer. *ACS Nano*, 2012, vol. 6 (10), pp. 8857–8867. DOI: 10.1021/nn302784m.

45. Umadevi D., Panigrahi S., Sastry G.N. Noncovalent interaction of carbon nanostructures. *Accounts of Chemical Research*, 2014, vol. 47 (8), pp. 2574–2581.

46. Vasileiou A.A., Docoslis A., Kontopoulou M., Xiang P., Ye Z. The role of non-covalent interactions and matrix viscosity on the dispersion and properties of LLDPE/MWCNT nanocomposites. *Polymer*, 2013, vol. 54 (19), pp. 5230–5240.

47. Nishio M. The CH/π hydrogen bond in chemistry. *Physical Chemistry Chemical Physics*, 2011, vol. 13 (31), pp. 13873–13900.

48. Waller M.P., Robertazzi A., Platts J.A., Hibbs D.E., Williams P.A. Hybrid density functional theory for π-stacking interactions: Application to benzenes, pyridines, and DNA bases. *Journal of Computational Chemistry*, 2006, vol. 27 (4), pp. 491–504.

49. Liu Z., Gao H., Wen S., Lin H., Chen X., Chen G. The influence of xylene content on the dispersion of graphene in aromatic petroleum resin by solution mixing. *Applied Surface Science*, 2021, vol. 567, p. 150718.

50. Krishnamoorthy K., Veerapandian M., Yun K., Kim S. The chemical and structural analysis of graphene oxide with different degrees of oxidation. *Carbon*, 2012, vol. 53, pp. 38–49.

51. Zhu B.Y., Murali S., Cai W., Li X., Suk J.W., Potts J.R., Ruoff R.S. Graphene and graphene oxide: Synthesis, properties, and applications. *Advanced Materials*, 2010, vol. 22, pp. 3906–3924.

52. Chen D., Feng H., Li J. Graphene oxide: Preparation, functionalization, and electrochemical applications. *Chemical Reviews*, 2012, vol. 112 (11), pp. 6027–6053.

53. Pei S., Cheng H.M. The reduction of graphene oxide. *Carbon*, 2011, vol. 50 (9), pp. 3210–3228.

54. Narayan J., Bezborah K. Recent advances in the functionalization, substitutional doping and applications of graphene/graphene composite nanomaterials. *RSC Advances*, 2024, vol. 14, pp. 13413–13444.

55. Lin J., Peng Z., Liu Y., Ruiz-Zepeda F., Ye R., Samuel E.L.G., Yacaman M.J., Yakobson B.I., Tour J.M. Laser-induced porous graphene films from commercial polymers. *Nature Communications*, 2014, vol. 5, pp. 1–12.

56. Ott A.K., Ferrari A.C. Raman spectroscopy of graphene and related materials. *Encyclopedia of Condensed Matter Physics*. Elsevier, 2024, pp. V2:233–V2:247.

57. Preston D.J., Mafra D.L., Miljkovic N., Kong J., Wang E.N. Scalable graphene coatings for enhanced condensation heat transfer. *Nano Letters*, 2015, vol. 15 (5), pp. 2902–2909.

Conflicts of Interest

The authors declare no conflict of interest.